Thermodynamic properties of supercritical *n-m* Lennard-Jones fluids and isochoric and isobaric heat capacity maxima and minima

Jonas Mairhofer[1] and Richard J. Sadus[2,a)]
[1]*Institut für Thermodynamik und Thermische Verfahrenstechnik, Universität Stuttgart, Pfaffenwaldring 9, 70569 Stuttgart, Germany*
[2]*Centre for Molecular Simulation, Swinburne University of Technology, P.O. Box 218 Hawthorn, Victoria 3122, Australia*

(Received 31 July 2013; accepted 25 September 2013; published online 15 October 2013)

Molecular dynamics simulations are reported for the thermodynamic properties of *n-m* Lennard-Jones fluids, where $n = 10$ and 12, and $m = 5$ and 6. Results are reported for the thermal expansion coefficient, isothermal and adiabatic compressibilities, isobaric and isochoric heat capacities, Joule-Thomson coefficient, and speed of sound at supercritical conditions covering a wide range of fluid densities. The thermodynamic criteria for maxima/minima in the isochoric and isobaric heat capacities are identified and the simulation results are also compared with calculations from Lennard-Jones equations of state. The Johnson *et al.* [Mol. Phys. **78**, 591 (1993)] equation of state can be used to reproduce all heat capacity phenomena reported [T. M. Yigzawe and R. J. Sadus, J. Chem. Phys. **138**, 194502 (2013)] from molecular dynamics simulations for the 12-6 Lennard-Jones potential. Significantly, these calculations and molecular dynamics results for other *n-m* Lennard-Jones potentials support the existence of C_p minima at supercritical conditions. The values of *n* and *m* also have a significant influence on many other thermodynamic properties. © *2013 AIP Publishing LLC*. [http://dx.doi.org/10.1063/1.4824626]

I. INTRODUCTION

Thermodynamic properties and phase behavior of fluids are directly linked to the nature of intermolecular interactions.[1] For example, theories of solid-liquid coexistence are commonly based on the observation that the structure of dense fluids is dominated by steep repulsive interaction between atoms or molecules.[2–5] The *n-m* Lennard-Jones (LJ) potential with $n = 12$ and $m = 6$ is a common starting point for both theoretical studies and molecular simulations.[6] In general it is adequate for atomic fluids, whereas modelling the behavior of molecules or monomers of polymer chains usually requires a potential with a softer repulsive part.[7]

A simple soft core potential can be obtained by replacing the $n = 12$ exponent in the 12-6 Lennard-Jones potential by a smaller integer. It has been found that varying the value of this exponent and, therefore the steepness of the main repulsive branch of the potential, significantly affects vapor-liquid equilibria,[7–10] the critical point,[8] and transport properties.[11–13] It also has a profound effect on solid-liquid coexistence.[14] In contrast, the effect of varying *n* on important thermodynamic properties such as the thermal expansion coefficient (α_p), isothermal (β_T) and adiabatic (β_S) compressibilities, isobaric (C_p) and isochoric (C_V) heat capacities, Joule-Thomson coefficient (μ_{JT}), and speed of sound (w_0) have not been widely studied. It is also rare to find an investigation of the role of *m* on either thermodynamic or other properties.

The fact that only a few thermodynamic properties can be observed directly from conventional molecular simulations partly explains the absence of data. In a microcanonical (*NVE*) ensemble simulation, which maintains a constant number of particles (*N*), volume (*V*), and total energy (*E*), the only directly observable thermodynamic quantities are the potential energy (*U*), pressure (*p*), and temperature (*T*). The calculation of other thermodynamic quantities requires the use of fluctuation formulas or equations of state.[15,16] Lustig[17] showed that it is possible to calculate all thermodynamic state variables from key derivatives obtained directly from either molecular dynamics (MD) or Monte Carlo (MC) simulations. The method, which was subsequently refined by Meier and Kabelac,[18] is based on the exact expressions for the thermodynamic state variables in the $NVE\vec{P}\vec{G}$ ensemble, which maintains both constant linear momentum ($\vec{P}$) and an additional quantity ($\vec{G}$) that is related to the initial position of the center of mass. The $NVE\vec{P}\vec{G}$ method has been successfully used to obtain the thermodynamic properties of a Gaussian core model fluid[19] and water.[20]

A pure fluid is in a supercritical state at temperatures and pressures above that of its critical point. Recently,[21] a MD investigation of the thermodynamic properties of supercritical 12-6 Lennard-Jones fluids reported maxima and minima values for both C_V and C_p. The existence of both minima and maxima for C_V is well-documented experimentally,[22–24] although they are not a universal feature of fluids. Similarly, many real fluids[22] have maxima in C_p. In contrast, the observation of minima in C_p is new. To the best of our knowledge, no previous simulation studies, theoretical calculations, or experimental work have reported C_p minima. The significance

a)Author to whom correspondence should be addressed. Electronic mail: rsadus@swin.edu.au

of this finding is that it provides an explanation for the terminal C_p value at high temperatures. Instead of being an isolated point, terminating a locus of heat capacity maxima, it is the point of transition linking loci of both heat capacity minima and maxima. The phenomenon is in some respect analogous to the critical point and the loci obey the same power law relationship as phase equilibria with an exponent of $\beta = 0.32$.

In this work, we make use of the $NVE\vec{P}\vec{G}$ method to determine α_p, β_T, β_S, C_p, C_V, μ_{JT}, and w_0 for *n-m* Lennard-Jones fluids. Our aim is to demonstrate how the thermodynamic properties vary with both *n* and *m*. We investigate the thermodynamic basis of the maxima and minima in both C_p and C_V and whether these phenomena are also observed for other *n-m* LJ fluids. The ability of LJ equations of state to predict thermodynamic maxima and minima is also determined.

II. MD SIMULATIONS

A. Intermolecular potentials

The *n-m* Lennard-Jones potential is[25]

$$u(r) = \varepsilon \left(\frac{n}{n-m}\right)\left(\frac{n}{m}\right)^{\left(\frac{m}{n-m}\right)}\left[\left(\frac{\sigma}{r}\right)^n - \left(\frac{\sigma}{r}\right)^m\right], \qquad (1)$$

where *r* is the interatomic separation, σ is the atomic diameter and ε is the well depth. We will consider potentials with $n = 10$ and 12 for which $m = 5$ or 6. For a given value of *m*, reducing the index *n* results in a wider attractive part and weaker repulsive force. Figure 1 compares the energies (Fig. 1(a)) and forces (Fig. 1(b)) of the 12-5 LJ and 10-6 LJ potentials relative to the 12-6 LJ potential. In both cases, attractive interactions increase and repulsion decreases at all interatomic separations. However, the changes observed for the 12-5 LJ potential are much greater than for the 10-6 LJ potential, particularly at larger separations. It should be noted that attributing *n* and *m* contributions to repulsion and attraction, respectively is only a convenient approximation. The continuous nature of the potential with respect to interatomic separation means that it is impossible to isolate either purely repulsive or purely attractive contributions. As *n* approaches infinity, the leading coefficient of Eq. (1) approaches ε and the *n-m* Lennard-Jones potential reaches the limiting case of a "hard-sphere + attractive term" potential.[8]

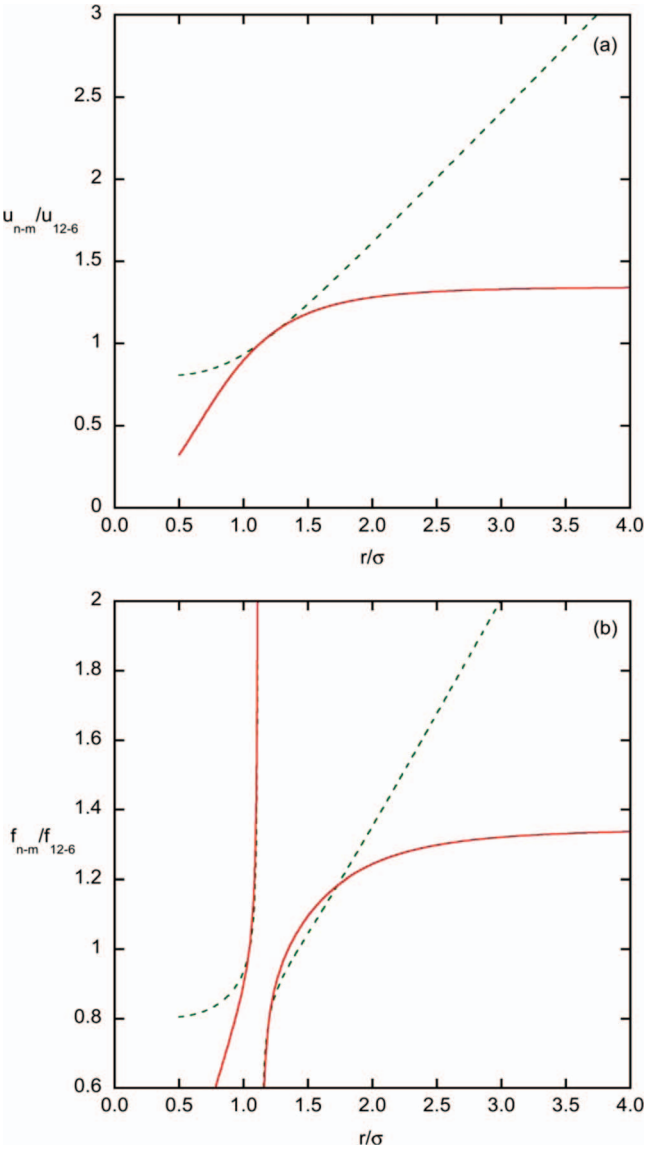

FIG. 1. Comparison of the (a) potential energy and (b) force as a function of intermolecular simulation for the 12-5 LJ (green broken line) and 10-6 (red line) LJ potentials relative to the 12-6 LJ potential. There are discontinuities in the ratios because the values for the 12-6 LJ potential become zero.

B. The *NVE$\vec{P}\vec{G}$* method

The $NVE\vec{P}\vec{G}$ ensemble simulations simply involve implementing a conventional $NVE\vec{P}$ simulation while keeping track of the volume derivatives of the intermolecular potential required for the evaluation of the thermodynamic quantities. The method has been discussed in detail in Refs. 17–21 and only a brief outline is given here. The fundamental equation of state for the system is defined by the entropy (*S*) postulate,[17,18] i.e.,

$$S(N, V, E, \vec{P}, \vec{G}) = k \ln \Omega(N, V, E, \vec{P}, \vec{G}), \qquad (2)$$

where $\Omega(N, V, E, \vec{P}, \vec{G})$ is the phase-space volume and *k* is the Boltzmann constant. The basic phase-space functions are then introduced as an abbreviation representing the derivatives of the phase-space volume with respect to the independent thermodynamic state variables

$$\Omega_{mn} = \frac{1}{\omega}\frac{\partial^{m+n}\Omega}{\partial E^m \partial V^n}, \qquad (3)$$

where ω is the phase-space density. A feature of the determination of the Ω terms is the evaluation of volume derivatives of the potential energy

$$\frac{\partial^n U}{\partial V^n} = \frac{1}{3^n V^n}\sum_{i=1}^{N-1}\sum_{j=i+1}^{N}\sum_{k=1}^{n} a_{nk}\, r_{ij}^k \frac{\partial^k u}{\partial r_{ij}^k}, \qquad (4)$$

where the coefficients a_{nk} are constructed using a recursion relation. All thermodynamic state variables are then expressible in terms of the phase-space function. The formulas for the thermodynamic state variables used in this work are summarized in Refs. 18–21.

C. Simulation details

The initial configuration for all simulations was an imperfect face centred cubic (fcc) lattice structure. The $NVE\vec{P}\vec{G}$ MD simulations were performed for a homogenous fluid of 1000 particles interacting via the *n-m* LJ potential. The normal conventions were used for the reduced density ($\rho^* = \rho\sigma^3$), temperature ($T^* = kT/\varepsilon$), potential energy ($U^* = U/N\varepsilon$), pressure ($p^* = p\sigma^3/\varepsilon$), heat capacities ($C^*_{P,V} = C_{P,V}/k$), compressibilities ($\beta^*_{T,S} = \beta_{T,S}\varepsilon/\sigma^3$), thermal expansion coefficient ($\alpha^*_P = \alpha_P\varepsilon/k$), speed of sound ($w^*_0 = w_0\sqrt{m/\varepsilon}$), where m is the mass of the particles, the Joule-Thomson coefficient ($\mu^*_{JT} = \mu_{JT}k/\sigma^3$), and time step ($\tau^* = [\varepsilon/m\sigma^2]^{1/2}\tau$). All quantities quoted in this work are in terms of these reduced quantities and the asterisk superscript will be omitted in the rest of the paper, with the exception of Eqs. (11) and (12).

The equations of motion were integrated using a five-value Gear predictor-corrector scheme[6,26] with $\tau = 0.001$. For each state point, simulation trajectories were run for 10×10^6 time steps with 8×10^6 time steps used to equilibrate the system. For the *n-m* LJ potentials, the cut-off radius was 6.5σ and conventional long-range corrections[6] were used for U and p, whereas the long-range corrections for the volume derivatives were calculated from the formulas reported by Meier and Kabalec.[18] In Fig. 2 and Figs. 6–11 error bars are not shown because, in most cases, the calculated statistical uncertainties of the data points are similar to the size of the symbols. Simulations were performed for $\rho = 0.1$–1.0 and various supercritical temperatures. Most of the data in the figures are for either $T = 1.6$ or $T = 3.0$. $T = 1.6$ is above the critical temperature[27] ($T = 1.312$) of the 12-6 LJ fluid, whereas $T = 3.0$ is a supercritical temperature for all the *n-m* LJ potentials studied here and as such it is a useful common temperature for the comparison between the potentials.

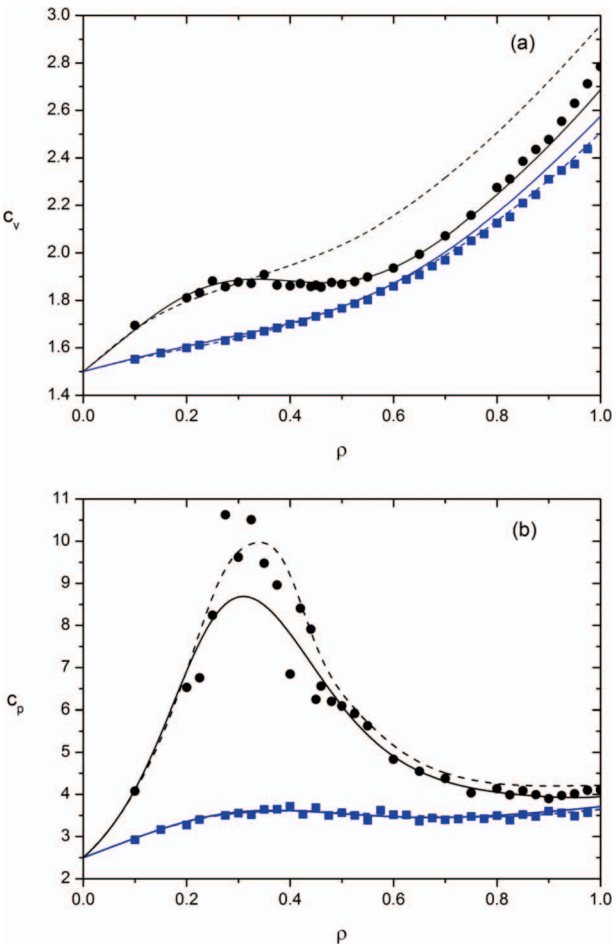

FIG. 2. Comparison of (a) C_V and (b) C_p simulation data for the 12-6 LJ potential at $T = 1.6$ (black circle, ●) and $T = 3.0$ (blue square, ■) with calculations using the Johnson (solid lines) and Mecke (broken lines) 12-6 LJ EoS.

III. CRITERIA FOR HEAT CAPACITY MAXIMA, MINIMA, AND EXTREMA

For a given isotherm at supercritical temperatures, maxima/minima in either C_V or C_p correspond to[21]

$$\left.\begin{aligned}\left(\frac{\partial C_{p,V}}{\partial V}\right)_{T>T_c,T\le T_E} &= 0\\ \left(\frac{\partial^2 C_{p,V}}{\partial V^2}\right)_{T>T_c,T<T_E} &\neq 0\end{aligned}\right\}, \tag{5}$$

where maxima and minima are observed when the second derivative is <0 and >0, respectively. The maxima/minima in the supercritical phase occurs at a temperature (T_M) greater than the critical temperature (T_c) but less than the temperature extreme (T_E) at which maxima and minima coincide. The temperature extreme occurs at a point of inflection characterized by[21]

$$\left.\begin{aligned}\left(\frac{\partial C_{p,V}}{\partial V}\right)_{T=T_E} &= 0\\ \left(\frac{\partial^2 C_{p,V}}{\partial V^2}\right)_{T=T_E} &= 0\\ \left(\frac{\partial^3 C_{p,V}}{\partial V^3}\right)_{T=T_E} &\neq 0\end{aligned}\right\}. \tag{6}$$

Using the thermodynamic relationship,[28,29]

$$\left(\frac{\partial C_V}{\partial V}\right)_T = T\left(\frac{\partial^2 p}{\partial T^2}\right)_V, \tag{7}$$

means that the criteria for observing maxima and minima in C_V are

$$\left.\begin{aligned}\left(\frac{\partial^2 p}{\partial T^2}\right)_{V_M} &= 0\\ \left(\frac{\partial^3 p}{\partial T^2 \partial V}\right) &\neq 0\end{aligned}\right\}. \tag{8}$$

To evaluate the criteria for maxima and minima in C_p, we make use of the following standard thermodynamic

relationships:[28,29]

$$\left.\begin{aligned} C_p &= C_V - T\left(\frac{\partial p}{\partial T}\right)_V^2 \Big/ \left(\frac{\partial p}{\partial V}\right)_T \\ \frac{\beta_T}{\alpha_p} &= \left(\frac{\partial T}{\partial p}\right)_V \\ \beta_T &= -\frac{1}{V}\left(\frac{\partial V}{\partial p}\right)_T \end{aligned}\right\}, \tag{9}$$

which transform Eq. (5) to

$$\left.\begin{aligned} &\left(\frac{\partial^2 p}{\partial T^2}\right)_{V_M} + 2\alpha_p V\left(\frac{\partial^2 p}{\partial V \partial T}\right) + \alpha_p^2 V^2\left(\frac{\partial^2 p}{\partial V^2}\right)_{T_M} = 0 \\ &\left(\frac{\partial^3 p}{\partial T^2 \partial V}\right) + 2\beta_T V\left(\frac{\partial^2 p}{\partial V \partial T}\right)^2 \\ &+ 2\alpha_p V\left(\left(\frac{\partial^3 p}{\partial V^2 \partial T}\right) + 2V\beta_T\left(\frac{\partial^2 p}{\partial V \partial T}\right)\left(\frac{\partial^2 p}{\partial V^2}\right)_{T_M}\right) \\ &+ \alpha_p^2 V^2\left(2V\beta_T\left(\frac{\partial^2 p}{\partial V^2}\right)_{T_M}^2 + \left(\frac{\partial^3 p}{\partial V^3}\right)_{T_M}\right) \neq 0 \end{aligned}\right\}. \tag{10}$$

When $\alpha_p = 0$, it is apparent from Eq. (9) that $\beta_T = 0$ which means that Eqs. (8) and (10) will be identical. A well-known example of $\alpha_p = 0$ is liquid water at its maximum density at a temperature of approximately 4 °C, which coincides with $C_V = C_p$. These circumstances do not occur at supercritical conditions.

The heat capacities and criteria for maxima/minima can be obtained by evaluating the necessary derivatives from an equation(s) of state (EoS). Several 12-6 LJ EoS have been proposed, some of which are compared in Ref. 30. Nicolas *et al.*[31] proposed an EoS based on molecular simulation data, which was subsequently updated by Johnson *et al.*[32] The Johnson *et al.*[32] EoS for a 12-6 LJ fluid is

$$p^* = \rho^* T^* + \sum_{i=1}^{8} a_i \rho^{*(i+1)} + e^{-3\rho^{*2}} \sum_{i=1}^{6} b_i \rho^{*(2i+1)}, \tag{11}$$

where the standard definitions for the reduced temperature, pressure, and density are used. The a and b parameters are empirical terms obtained from fitting[31] the equation of state to a wide range of simulation data. Mecke *et al.*[33] proposed that the Helmholtz function (A), and hence the EoS for the 12-6 LJ fluid could be obtained from

$$\left.\begin{aligned} \frac{A}{NkT} &= \frac{(4\xi - 3\xi^2)}{(1-\xi)^2} + \sum_i c_i (T^*/T_c^*)^{m_i} (\rho^*/\rho_c^*)^{n_i} \exp[p_i (\rho^*/\rho_c^*)^{q_i}] \\ \xi &= -0.1617(\rho^*/\rho_c^*)[0.689 + 0.311(T^*/T_c^*)^{0.3674}]^{-1} \end{aligned}\right\}. \tag{12}$$

In common with the Johnson *et al.*[32] approach the m, n, p, q, and c terms were obtained from optimizing agreement with molecular simulation data. Hereafter, we will refer to the Johnson *et al.*[32] and Mecke *et al.*[33] EoS simply as the Johnson and Mecke EoS, respectively.

IV. RESULTS AND DISCUSSION

A. Observation of heat capacity maxima and minima

Yigzawe and Sadus[21] reported simulation data showing minima in C_p for the 12-6 LJ potential. This behavior was unexpected because it had not been observed previously from theory, molecular simulation or experiment. The absence of experimental data may indicate that it is an artefact of the 12-6 Lennard-Jones potential. However, the well-documented ability of the 12-6 LJ potential to at least qualitatively reproduce many other experimentally observed phenomena of simple fluids suggests that this explanation is unlikely. Alternatively, the absence of experimental data could be attributed to the fact that the minimum is very shallow in comparison to the very large C_p maximum and it occurs at densities and pressures that are outside of the normal range of experimental measurements. In view of this, it is of interest to determine whether a 12-6 LJ EoS can reproduce the phenomenon.

The definition of the maxima/minima criteria (Eqs. (8) and (10)) has some interesting consequences for both the behavior of real fluids and the accuracy of EoS prediction. Many EoS, most notably the van der Waals equation and other widely used "hard sphere + attractive term" EoS[34] cannot predict maxima/minima in C_V because criteria (8) are satisfied at all densities, temperatures, and pressures. However, the same EoS that fails to predict the C_V maxima/minima could predict these phenomena for C_p because criteria (10) contain additional terms that are generally not invariant for the EoS. These considerations also apply to real fluids, which explain the diversity of phenomena observed experimentally. For example, a real fluid with a C_V maximum is likely to have a C_p maximum, whereas a C_p maximum does not guarantee a C_V maximum.

We tested both the Johnson (Eq. (11)) and Mecke (Eq. (12)) EoS. Figure 2(a) compares the C_V results obtained from the two EoS with simulation data at temperatures of $T = 1.6$ and 3.0. There is very good agreement with simulation data for both EoS at $T = 3.0$. At the lower temperature of $T = 1.6$, the simulation data for C_V display both a maximum and minimum. The Johnson EoS calculations faithfully reproduce this behavior and the overall agreement is very good at all densities. In contrast, the Mecke EoS predicts neither the maximum nor

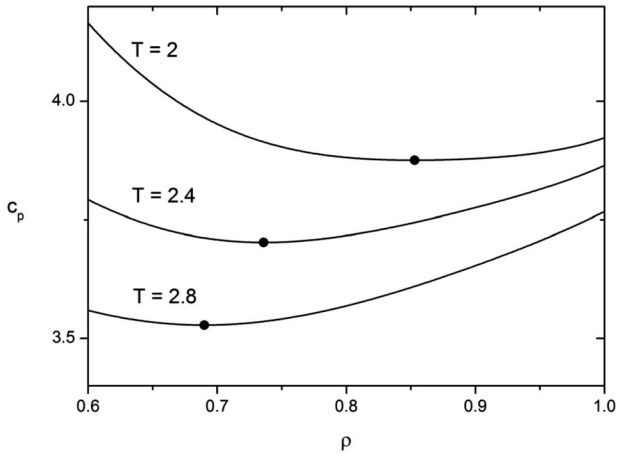

FIG. 3. Close-up of the C_p curve as a function of density showing the minima (●) predicted by the Johnson EoS at $T = 2$, 2.4, and 2.8.

minimum and the agreement is poor at all densities. The corresponding results for C_p are illustrated in Fig. 2(b). At $T = 3.0$, the results for the two EoS are almost indistinguishable. At $T = 1.6$, the simulation data show a pronounced maximum at moderate densities and a very shallow minimum at high densities. Both EoS predict a C_p maximum. The magnitude of C_p predicted by the Mecke EoS is closer to the simulation data than the Johnson EoS. Although it is difficult to resolve on the scale given in Fig. 2(b), the Johnson EoS also has a minimum in C_p whereas the Mecke EoS does not.

The apparently inconsistent results for the Mecke EoS, that is its failure to predict C_v maxima/minima while displaying a C_p maximum can be explained in terms of the thermodynamic criteria for these phenomena (Eqs. (8) and (10)). The absence of C_V maxima/minima does not preclude C_p maxima/minima because of the additional terms (Eq. (10)) that are involved for such phenomena.

Yigzawe and Sadus[21] noted that it is difficult to accurately identify C_p minima because there is considerable scatter in the simulation data and, unlike the C_p maxima, the minima is very shallow. EoS calculations are potentially helpful because the issue of data scatter does not arise. The Mecke EoS qualitatively reproduced the maxima in C_p but C_p minima could not be found irrespective of temperature or density. In contrast, the Johnson EoS reproduced all the phenomena observed in the simulations, including the C_p minima (see Fig. 3). The inability of the Mecke EoS to predict the C_p minima compared with successful calculations obtained for the Johnson EoS probably reflects the differences in parameterization. In particular, Mecke *et al.*[33] based their parameterisation on the Carnahan-Starling[35] hard-sphere term. The criteria for the C_p maxima/minima would preclude these phenomena from being observed for many EoS. This is particularly the case for EoS based on hard-sphere approximations.

The maxima and minima predicted by the Johnson EoS are compared with simulation data[21] in Fig. 4(a), which also shows the regions of vapor-liquid[36] and solid-liquid[37] coexistence for the 12-6 LJ fluid. There is reasonable agreement between EoS calculations and simulation data for C_v, although the calculated extreme point ($T_E = 1.696$, $\rho_E = 0.389$, $p_E = 0.436$) is higher than obtained from simulation[21] ($T_E = 1.667$, $\rho_E = 0.382$, $p_E = 0.384$). The agreement between simulation data and EoS calculations for C_p is poor, with the calculated extreme point ($T_E = 6.234$, $\rho_E = 0.557$, $p_E = 7.501$) occurring at a much higher temperature than obtained from simulation[21] ($T_E = 2.905$, $\rho_E = 0.539$, $p_E = 2.550$). However, it should be emphasised that the important aspect of this comparison is that it independently confirms both the existence of C_p minima and the transition between C_p minima and maxima obtained from simulations.

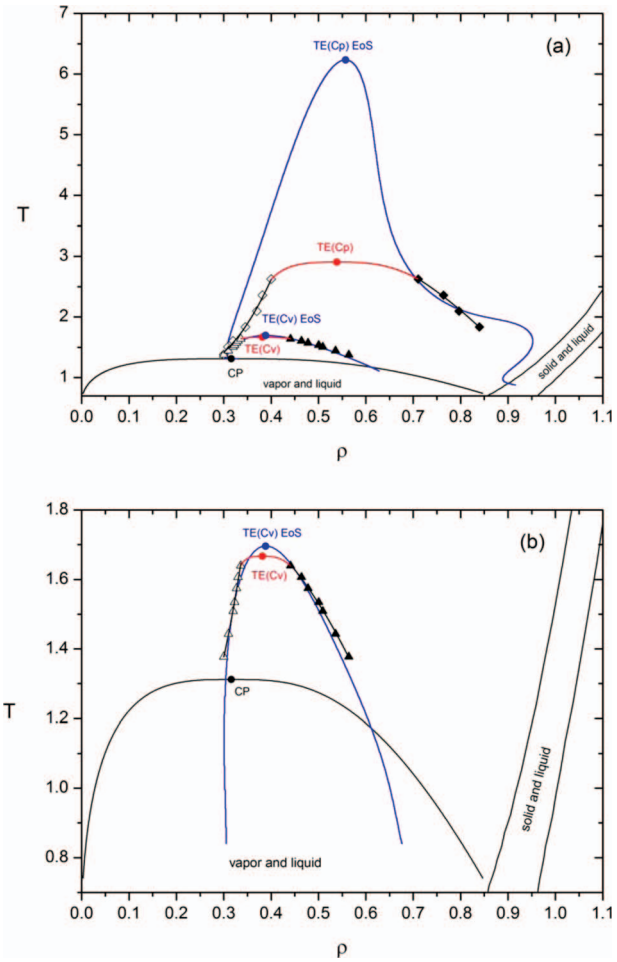

FIG. 4. (a) Comparison of simulation data (Ref. 21) for temperature-density behavior of the supercritical maxima (open symbols) and minima (closed symbols) of C_p(◇,◆), C_V(△, ▲) for the 12-6 Lennard-Jones fluid with calculations obtained from the Johnson EoS (blue solid lines). The vapor-liquid (—, Ref. 37) and solid-liquid (—, Ref. 36) coexistence curves are also illustrated. The red lines linking the maxima and minima heat capacity data were obtained by fitting the data using the phase coexistence power relationship with an exponent of $\beta = 0.32$. The vapor-liquid critical point (●, CP), and temperature extremes (red circle, ●, TE) for both C_V and C_p are identified. (b) A close-up view of the C_V data.

The comparison between simulation and calculations for C_V is shown in more detail in Fig. 4(b). One reason for the discrepancy between the simulation data and calculations is that the simulation data obey the non-classical value for the power law exponent ($\beta = 0.32$), whereas the EoS data follow the classical value ($\beta = 0.5$) common to conventional (mean field) equations of state. This suggests that the agreement could be improved by adding cross-over[38] features into

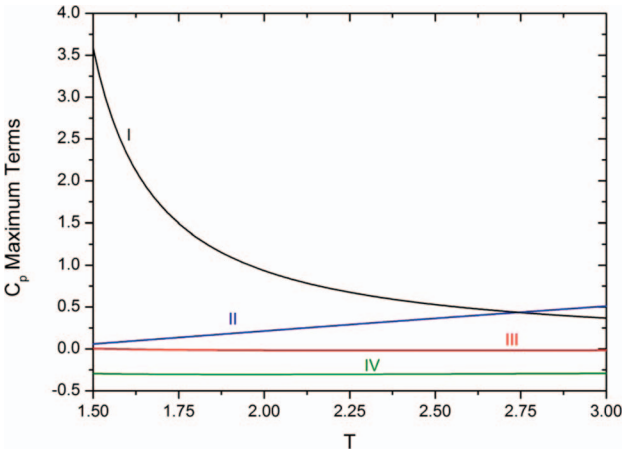

FIG. 5. Comparison of the various contributions to Eq. (10) obtained from the Johnson EoS in the vicinity of a C_p maximum (T = 2, $\rho = 0.325$). Illustrated are values of (i) α_p (black line), (ii) $(\partial^2 p/\partial V^2)_T$(blue line), (iii) $(\partial^2 p/\partial T^2)_V$ (red line), and (iv) $(\partial^2 p/\partial V \partial T)$ (green line). The calculations were performed for a constant value of $\rho = 0.325$, corresponding to density of the C_p maximum.

the Johnson 12-6 LJ EoS. Figure 4(b) also shows that the EoS calculations extend into the two-phase vapor-liquid region. Phenomena in this region are either metastable or unstable and it is not surprising that some pressures and heat capacities calculated there are negative. The EoS C_p data (not illustrated) extend into both the two-phase liquid-vapor and solid-liquid regions.

It is of interest to compare the relative contributions of the various thermodynamic quantities used in the C_p maxima/minima criteria (Eq. (10)). The various quantities obtained from the Johnson EoS in the vicinity of a C_p maximum are compared in Fig. 5. It is apparent that both α_p and $(\partial^2 p/\partial V^2)_T$ are much more temperature-dependent than the remaining terms and as such have the most important influence on the location of the C_p maximum. The value of α_p diverges in the vicinity of the critical temperature ($T = 1.312$) whereas $(\partial^2 p/\partial V^2)_T$ becomes zero.

B. Isochoric and isobaric heat capacities

Simulation results for C_V and C_p for the 12-6, 10-6, and 12-5 LJ potentials are illustrated in Figure 6 and a comparison is given for the 12-6 fluid obtained from the Mecke and Johnson EoS. It is noteworthy that at $T = 3.0$ neither the value of n nor m significantly affects C_V, which appears independent of both exponents at all densities (Fig. 6(a)). This probably reflects the fact that, for all the LJ potentials, $T = 3.0$ is above the T_E value for C_V. In contrast, C_p is sensitive to both n and m (Fig. 6(b)). Reducing the value of n from 12 to 10 results in a noticeable increase in the C_p maximum; however, the most significant increase occurs when m is reduced from 6 to 5. The scatter in the simulation data makes it difficult to draw definite conclusion regarding the effect on the minima.

Freasier *et al.*[39] interpreted the occurrence of C_V minima and maxima in terms of the interplay between molecular aggregation, caging, and soft-core repulsion. They attributed the C_V maxima at moderate densities as a transition between simple aggregation and caging effects whereas the C_V minimum was attributed to the increasing influence of soft-core penetration on the caged particles with increasing density. The C_V maximum requires the intermolecular potential to have an attractive well and it is not observed in purely repulsive systems. Particles interacting without some soft repulsion do not display a C_V minimum. Our results appear consistent with this interpretation. Based on this interpretation, the absence of C_V minima in Fig. 6(a) can be attributed to the effect of temperature dominating any soft-core repulsion. Freasier *et al.*[39] did not consider the influences on C_p but the widening of the potential well when $n = 5$ appears to be directly linked to an increase in C_p maxima.

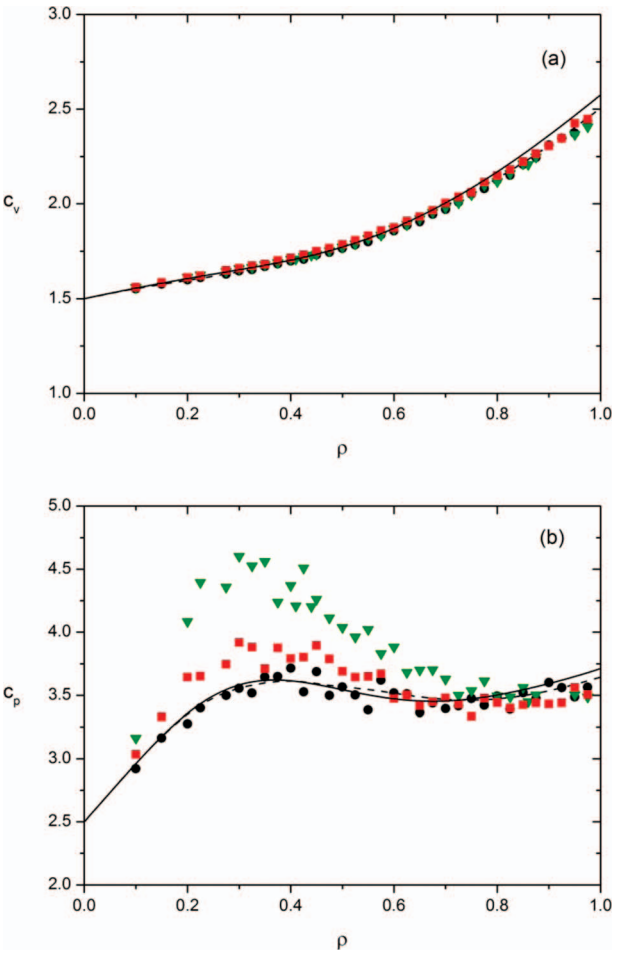

FIG. 6. Molecular simulation data for (a) C_V and (b) C_p obtained for the 12-6 (black circle, ●), 10-6 (red square, ■), and 12-5 (green triangle, ▼) LJ potentials at $T = 3.0$. Calculations for the Johnson (solid lines) and Mecke (broken lines) 12-6 LJ EoS are also illustrated.

C. Adiabatic and isothermal compressibilities

Values of β_S and β_T are illustrated in Fig. 7. At high densities ($\rho > 0.5$) the results for β_S for the various potentials are almost indistinguishable from each other. Reducing n from 12 to 10 results in a modest increase in β_S at lower densities, however a greater change is observed when m is reduced from 6 to 5. Nonetheless, the changes are relatively small. The same general trends are observed for β_T; however, the magnitude of

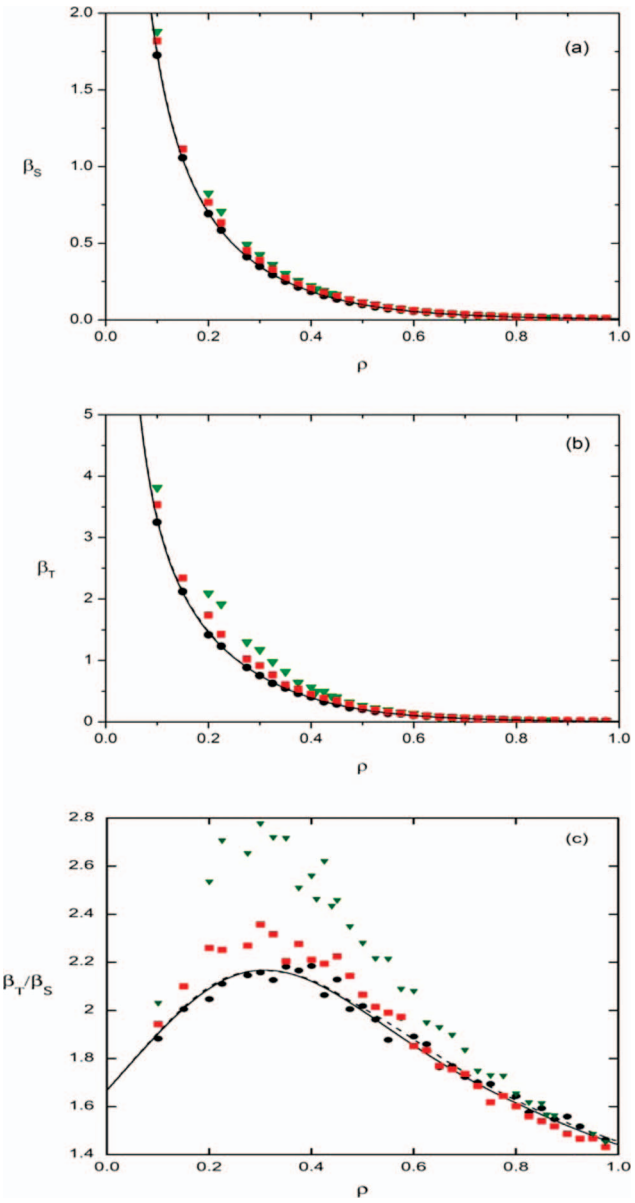

FIG. 7. Molecular simulation data for (a) β_S, (b) β_T, and (c) β_T/β_S obtained for the 12-6 (black circle, ●), 10-6 (red square, ■), and 12-5 (green triangle, ▼) LJ potentials at $T = 3.0$. Calculations for the Johnson (solid lines) and Mecke (broken lines) 12-6 LJ EoS are also illustrated.

the changes is considerably greater. The value of C_p is related to β_S and β_T via the following thermodynamic relationship:[27]

$$C_p = C_V \frac{\beta_T}{\beta_S}. \tag{13}$$

The β_T/β_S ratio as a function of density is illustrated in Fig. 7(c). In this example, the β_T/β_S ratio exhibits a maximum, which contributes to the C_p maximum. If C_V has a maximum, the existence of a maximum in the β_T/β_S ratio will magnify the C_p maximum, which partly explains the much larger maximum observed for C_p compared with C_V. The data in Fig. 7(c) also indicate that the maximum for the β_T/β_S ratio and therefore the C_p maximum is much larger for the 12-5 LJ potential than either the 10-6 LJ or 12-6 LJ potentials.

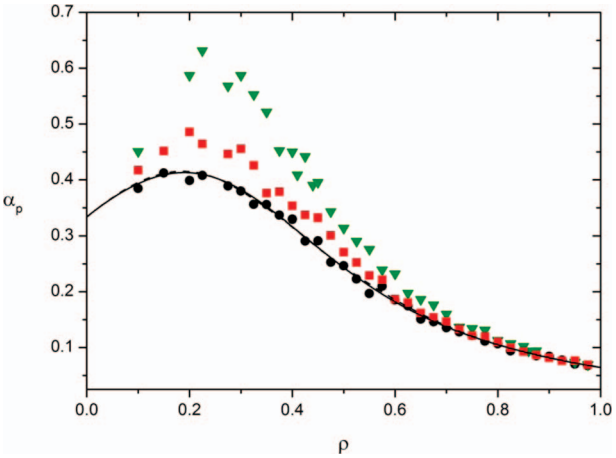

FIG. 8. Molecular simulation data for α_p obtained for the 12-6 (black circle, ●), 10-6 (red square, ■), and 12-5 (green triangle, ▼) LJ potentials at $T = 3.0$. Calculations for the Johnson (solid lines) and Mecke (broken lines) 12-6 LJ EoS are also illustrated.

D. Thermal expansion coefficient

In common with C_V and C_p, α_p exhibits maxima in the supercritical phase. This can be attributed to its connection to heat capacities via the following thermodynamic relationship:[29]

$$\alpha_p = \beta_S \frac{C_p}{C_V} \left(\frac{\partial p}{\partial T} \right)_V. \tag{14}$$

Simulation α_p data for the various potentials are illustrated in Fig. 8, which shows a maximum value in all cases. The trends are consistent with those observed for other thermodynamic properties, namely that reducing either the value of n or m increases the maximum but changing m has a much greater impact.

E. Joule-Thomson coefficient

Values of μ_{JT} for the LJ potentials are illustrated in Fig. 9 as functions of density. At low densities ($\rho < 0.5$),

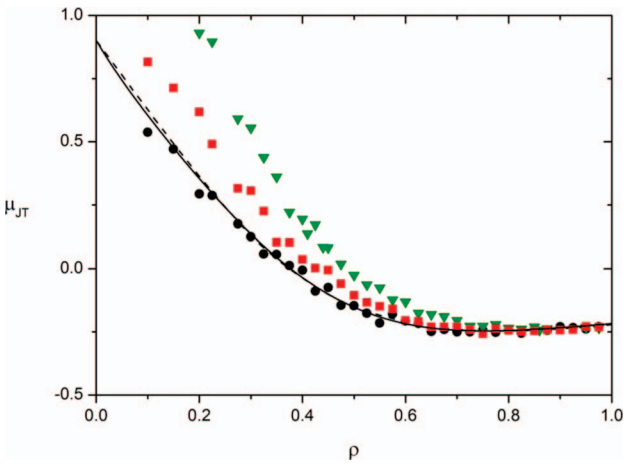

FIG. 9. Molecular simulation data for μ_{JT} obtained for the 12-6 (black circle, ●), 10-6 (red square, ■), and 12-5 (green triangle, ▼) LJ potentials at $T = 3.0$. Calculations for the Johnson (solid lines) and Mecke (broken lines) 12-6 LJ EoS are also illustrated.

μ_{JT} is sensitive to both the value of n and m, with m having the greatest impact. The μ_{JT} values for the LJ fluid decrease with increasing density along the isotherm, attaining a negative value at high densities. This means that there is an inversion curve (i.e., locus of $\mu_{JT} = 0$) for the LJ fluid. To obtain the inversion curve, we first calculated the density at which μ_{JT} is zero for each of the isotherms by finding the root of a polynomial fitted to simulation results of μ_{JT} in the vicinity of the density where the change of sign occurs. We then determined the corresponding value of the pressure at that density for each of the isotherms. This was achieved by finding the best fit of a polynomial for the simulated pressures and using it to calculate the pressure at each of the densities where $\mu_{JT} = 0$.

The inversion curve for the various potentials is illustrated in Fig. 10. Fig. 10(a) indicates that for a given density, either reducing n or m will result in a substantial increase in the inversion temperature, with m having the greatest influence. The effect on pressure is less dramatic (Fig. 10(b)), with the inversion curve being extended slightly to higher pressures.

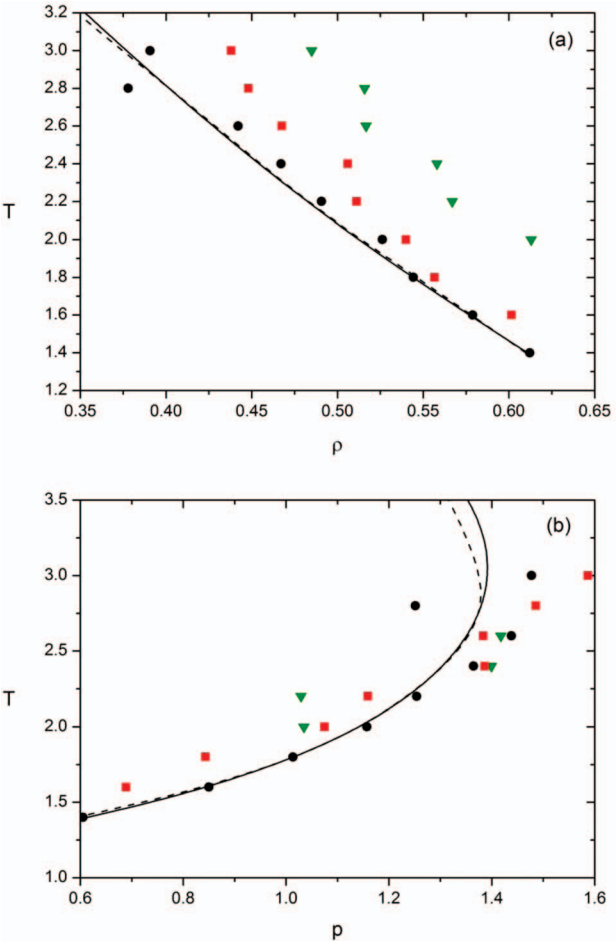

FIG. 10. Molecular simulation data for the (a) temperature-density and (b) temperature-pressure behavior of the Joule-Thomson inversion curve obtained for the 12-6 (black circle, ●), 10-6 (red square, ■), and 12-5 (green triangle, ▼) LJ potentials at $T = 3.0$. Calculations for the Johnson (solid lines) and Mecke (broken lines) 12-6 LJ EoS are also illustrated.

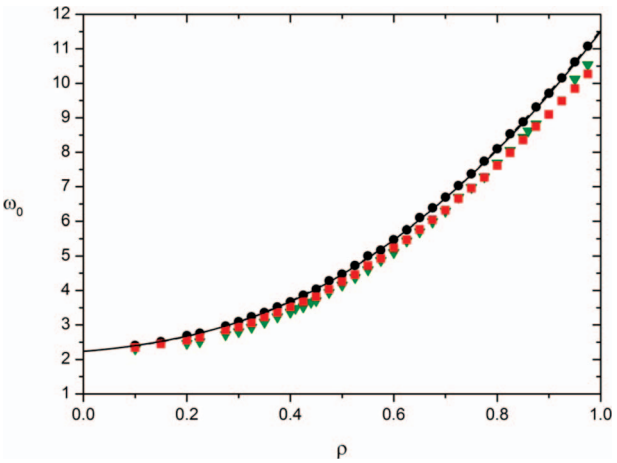

FIG. 11. Molecular simulation data for w_0 obtained for the 12-6 (black circle, ●), 10-6 (red square, ■), and 12-5 (green triangle, ▼) LJ potentials at $T = 3.0$. Calculations for the Johnson (solid lines) and Mecke (broken lines) 12-6 LJ EoS are also illustrated.

F. Speed of sound

The zero frequency speed of sound as a function of temperature at different constant densities is illustrated in Fig. 11. It is apparent from the comparison given in Fig. 11, that at $\rho > 0.2$, both the 10-5 and 12-5 LJ potentials result in reduced values of w_0. However, the reduction is relatively small compared with the effect of changing the exponent for other properties. This is consistent with the dependence of w_0 on β_S, via the thermodynamic relationship[28]

$$w_0^2 = \frac{V}{M\beta_s}, \tag{15}$$

where M is the total mass of the system. The influence of n and m on β_S (Fig. 7) is relatively small, which is also reflected in the values of w_0.

In Fig. 2 and Figs. 6–11 comparisons are given with calculations from both the Johnson and Mecke EoS. It is apparent from these comparisons that both EoS generally yields good agreement with the 12-6 LJ simulation data. This is to be expected as both equations were fitted to simulation data. However, for reasons discussed above, the notable exception is the failure of the Mecke EoS to predict the C_V maxima/minima (Fig. 2).

V. CONCLUSIONS

The thermodynamic criteria for maxima/minima in the isochoric and isobaric heat capacities have been identified. The Johnson EoS can be used to qualitatively reproduce all heat capacity phenomena obtained from MD simulations for the 12-6 LJ potential. Significantly, these calculations support the existence of C_p minima at supercritical conditions. In contrast the Mecke EoS fails to predict C_V minima and although C_p maxima are predicted, C_p minima are not. This can be partly explained by the use of a hard-sphere term in the Mecke EoS. Many "hard sphere + attractive term" EoS are unlikely to predict the full range of heat capacity behavior because key thermodynamic derivatives are invariant under all conditions.

The existence of C_p minima from both MD simulation data and Johnson EoS calculations suggest that it is worthwhile to attempt to identify this behavior from experiments on real fluids.

The MD results for the 12-6, 12-5, 10-6 LJ potentials indicate that thermodynamic properties such as α_p, β_T, C_p, and μ_{JT} are very sensitive to a change in the value of n from 12 to 6 and m from 6 to 5, with the value of the m exponent having a particularly noticeable impact. In comparison with the 12-6 LJ potential, considerably larger C_p and C_V maxima are observed for both the 12-5 and 12-10 LJ potentials. Reducing either n or m significantly affects the Joule-Thomson inversion curve by increasing the inversion temperature and pressure. In contrast, varying the potential's exponents has a relatively small effect on both w_0 and β_S.

ACKNOWLEDGMENTS

We thank the National Computing Infrastructure (NCI) for an allocation of computing time.

[1]C. G. Gray and K. E. Gubbins, *Theory of Molecular Fluids Vol. 1: Fundamentals* (Clarendon Press, Oxford, 1984); J.-P. Hansen and I. R. McDonald, *Theory of Simple Liquids*, 2nd ed. (Academic Press, London, 1986); A. E. Mather, R. J. Sadus, and E. U. Franck, J. Chem. Thermodyn. **25**, 771 (1993); G. Marcelli and R. J. Sadus, J. Chem. Phys. **112**, 6382 (2000).
[2]D. Frenkel and J. P. McTague, Ann. Rev. Phys. Chem. **31**, 491 (1980).
[3]J. A. Barker and D. Henderson, J. Chem. Phys. **47**, 4714 (1967).
[4]J. D. Weeks, D. Chandler, and H. C. Andersen, J. Chem. Phys. **54**, 5237 (1971).
[5]H. C. Longuet-Higgins and B. Widom, Mol. Phys. **8**, 549 (1964).
[6]R. J. Sadus, *Molecular Simulation of Fluids: Theory, Algorithms, and Object-Orientation* (Elsevier, Amsterdam, 1999); R. J. Sadus, Mol. Phys. **87**, 979 (1996).
[7]H. Meyer, O. Biermann, R. Faller, D. Reith, and F. Müller-Plathe, J. Chem. Phys. **113**, 6264 (2000).
[8]H. Okumura and F. Yonezawa, J. Chem. Phys. **113**, 9162 (2000).
[9]I. Charpentier and N. Jakse, J. Chem. Phys. **123**, 204910 (2005).
[10]K. Kiyohara, T. Spyriouni, K. E. Gubbins, and A. Z. Panagiotopoulos, Mol. Phys. **89**, 965 (1996).
[11]D. Heyes and J. Powles, Mol. Phys. **95**, 259 (1998).
[12]D. Heyes, G. Rickayzen, and A. Brańka, Mol. Phys. **102**, 2057 (2004).
[13]P. A. Gordon, J. Chem. Phys. **125**, 014504 (2006).
[14]A. Ahmed and R. J. Sadus, J. Chem. Phys. **131**, 174504 (2009).
[15]J. L. Lebowitz, J. K. Percus, and L. Verlet, Phys. Rev. **153**, 250 (1967).
[16]P. S. Y. Cheung, Mol. Phys. **33**, 519 (1977).
[17]R. Lustig, J. Chem. Phys. **100**, 3048 (1994).
[18]K. Meier and S. Kabelac, J. Chem. Phys. **124**, 064104 (2006).
[19]P. Mausbach and R. J. Sadus, J. Chem. Phys **134**, 114515 (2011).
[20]T. M. Yigzawe and R. J. Sadus, J. Chem. Phys. **138**, 044503 (2013).
[21]T. M. Yigzawe and R. J. Sadus, J. Chem. Phys. **138**, 194502 (2013).
[22]*Heat Capacities: Liquids, Solutions and Vapours*, edited by E. Wilhelm and T. Letcher (The Royal Society of Chemistry, Cambridge, 2010).
[23]A. I. Abdulagatov, G. V. Stepanov, I. M. Abdulagatov, A. E. Ramaznova, and G. S. Alidultanova, Chem. Eng. Commun. **190**, 1499 (2003).
[24]N. G. Polikhronidi, I. M. Abdulagotov, R. G. Butyrova, G. V. Stepanov, J. T. Wu, and E. E. Ustuzhanin, Int. J. Thermophys. **33**, 185 (2012).
[25]Eq. (1) can be alternatively identified as the *n-m* Mie potential with an attribution to G. Mie, Ann. Phys. **11**, 657 (1903), although Mie's use of different exponents is limited. The first systematic investigation of the effect of different n and m exponents on the properties of a fluid can be traced to J. E. Jones (later known as J. E. Lennard-Jones), Proc. R. Soc. London, Ser. A **106**, 463 (1924). The origin of the potential is discussed by J. S. Rowlinson, *Cohesion: A Scientific History of Intermolecular Forces* (Cambridge University Press, Cambridge, 2002). The descriptions *n-m* Mie potential and *n-m* Lennard-Jones potential refer to the same entity and as such are completely interchangeable. In this work, the latter terminology is used exclusively.
[26]C. W. Gear, *Numerical Initial Value Problems in Ordinary Differential Equations* (Prentice-Hall, Englewood Cliffs, NJ, 1971).
[27]J. J. Potoff and A. Z. Panagiotopoulos, J. Chem. Phys. **109**, 10914 (1998).
[28]J. S. Rowlinson, *Liquids and Liquid Mixtures*, 2nd ed. (Butterworths, London, 1969).
[29]A. Münster, *Classical Thermodynamics*, translated by E. S. Halberstadt (Wiley, London, 1970).
[30]Đ. Plačkov and R. J. Sadus, Fluid Phase Equilib. **134**, 77 (1997).
[31]J. J. Nicolas, K. E. Gubbins, W. B. Streett, and D. J. Tildesley, Mol. Phys. **37**, 1429 (1979).
[32]J. K. Johnson, J. A. Zollweg, and K. E. Gubbins, Mol. Phys. **78**, 591 (1993).
[33]M. Mecke, A. Müller, J. Winkelmann, J. Vrabec, J. Fischer, R. Span, and W. Wagner, Int. J. Thermophys. **17**, 391 (1996).
[34]R. J. Sadus, J. Chem. Phys. **115**, 1460 (2001); Y. S. Wei, and R. J. Sadus, AIChE J. **46**, 169 (2000); R. J. Sadus, J. Phys. Chem. **99**, 12363 (1995).
[35]N. F. Carnahan and K. E. Starling, J. Chem. Phys. **51**, 635 (1969).
[36]A. Ahmed and R. J. Sadus, J. Chem. Phys. **133**, 124515 (2010).
[37]D. Kofke, J. Chem. Phys. **98**, 4149 (1993).
[38]S. B. Kiselev and J. F. Ely, Fluid Phase Equilib. **174**, 93 (2000).
[39]B. C. Freasier, C. E. Woodward, and R. J. Bearman, J. Chem. Phys. **105**, 3686 (1996); **106**, 10318 (1997).